Integrated Effects of Site Hydrology and Vegetation on Exchange Fluxes and Nutrient Cycling at a Coastal Terrestrial-Aquatic Interface

Bing Li[1], Zhi Li[1], Jianqiu Zheng[1], Peishi Jiang[1], James Holmquist[3], Peter J. Regier[1], Glenn E. Hammond[1], Nicholas D. Ward[1], Allison Myers-Pigg[1], Roy Rich[3], Wei Huang[2], Theresa A. O'Meara[2], Stephanie C. Pennington[1], Patrick Megonigal[3], Vanessa L Bailey[1], Xingyuan Chen[1]

[1]Pacific Northwest National Laboratory, Richland, WA, USA 99352.
[2]Oak Ridge National Laboratory, Oak Ridge, TN, USA 37830.
[3]Smithsonian Environmental Research Center, Edgewater, MD, USA 21037.

Key Points:

- Tidal elevations, precipitation, and evapotranspiration interact to control dynamic exchange fluxes across the coastal terrestrial aquatic interface.
- Integrated hydrobiogeochemical modeling reveals significant variability in redox conditions along the gradient of upland, transition, and wetland to the open water.
- The high uncertainty in microbial-remediated aerobic respiration rates has a significant impact on modeling the carbon cycling in coastal regions.

Corresponding author: Xingyuan, Chen, `Xingyuan.Chen@pnnl.gov`

Abstract

The complex interactions among soil, vegetation, and site hydrologic conditions driven by precipitation and tidal cycles control the biogeochemical transformations and bi-directional exchange of carbon and nutrients across the terrestrial–aquatic interfaces (TAIs) in coastal regions. This study uses a highly mechanistic model, Advanced Terrestrial Simulator-PFLOTRAN, to explore how these interactions affect exchanges of materials and carbon and nitrogen cycling along a TAI transect in the Chesapeake Bay region that spans zones of open water, coastal wetland, and upland forest. We designed several simulation scenarios to parse the effects of the individual controlling factors and the sensitivity of carbon cycling to reaction rate constants derived from laboratory experiments. Our simulations revealed a hot zone for carbon cycling under the transition zones between the wetland and the upland. Evapotranspiration is found to enhance the exchange fluxes between the surface and subsurface domains, resulting in a higher dissolved oxygen concentration in the TAI. The transport of organic carbon derived from plant leaves and roots provides an additional source of organic carbon for the aerobic respiration and denitrification processes in the TAI. The reaction rate variability mediated by microbial activities, plays a dominant role in controlling the heterogeneity and dynamics of the simulated redox conditions. This modeling-focused exploratory study enabled us to better understand the complex interactions of various system components at the TAIs that control the hydro-biogeochemical processes, an important step towards representing coastal ecosystems in larger-scale Earth system models.

Plain Language Summary

The hydrological environment of vegetated coastal ecosystems is directly influenced by rainfall and seawater flooding, which mediates biogeochemical processes within these areas. However, the specific effects of dynamic rainfall and flooding on oxidation-reduction conditions in these complex terrestrial-aquatic interfaces (TAIs) are poorly understood, especially when considering the ecological processes of above-ground plants. To address this gap, this study used integrated process-based models, the Advanced Terrestrial Simulator and PFLOTRAN, to examine the effects of hydrological and ecological controls on biogeochemical reactions and exchange fluxes across a TAI transect spanning from a coastal upland forest and saltmarsh to the open seawater. Our numerical experiments showed that spatio-temporally dynamic surface–subsurface exchange fluxes and the spatial extent of oxic subsurface zones within the TAIs are significantly influenced by the mixing of different waters. The interface between the oxic and anoxic zones shifts in response to periodic fluctuations in tidal elevations as higher tides drive more oxygenated water towards the TAI. Meanwhile, vegetation evapotranspiration removes more water from the subsurface during warm summer months. Soil-dependent reaction rate constants have a large effect on the modeled reactions. A higher aerobic respiration rate will result in larger hypoxic and anoxic zones because the dissolved oxygen is consumed more quickly. Our modeling-based study provided insights into the mechanisms that control the exchange fluxes and carbon and nitrogen cycling at coastal TAIs, which can be used to inform potential management strategies to mitigate the impacts of climate change on these ecosystems.

1 Introduction

Coastal terrestrial–aquatic interfaces (TAIs) are known to disproportionately regulate ecosystem and biogeochemical functions that are critical for the health of both terrestrial and aquatic ecosystems [*Bailey et al.*, 2017a; *Enguehard et al.*, 2022; *Bauer et al.*, 2013; *Bianchi et al.*, 2018; *Erickson III et al.*, 2015]. Hydrologic, biogeochemical, and ecological processes interact along the gradient of coastal uplands (e.g., forests and grasslands), wetlands, and surface waters, affecting the distribution and cycling of dissolved organic carbon (DOC), nitrogen and oxygen [*Thorne and Williams*, 1997; *Costanza et al.*, 1997; *Mitsch and Gosselink*, 2007; *Assessment*, 2005; *Cowardin et al.*, 1979; *Chmura et al.*, 2003; *Michael et al.*, 2005]. Developing a mechanistic understanding of the exchange fluxes and nutrient cycling at coastal TAIs is critical for explicitly representing them in Earth system models (ESMs) to more accurately quantify global carbon budget and evaluate ecosystem resiliency and resistance to climate changes [*Kolka et al.*, 2021; *Tank et al.*, 2018; *Casas-Ruiz et al.*, 2023; *Ward et al.*, 2020; *Regier et al.*, 2021].

Climate and environmental changes such as sea level rise, storm surge, and flooding exert significant effects on the transport and mixing of reactants within coastal wetlands by shifting the hydrologic regimes [*Erwin*, 2009; *Robinson et al.*, 2018; *Paerl et al.*, 2019]. For example, rising seawater carries more oxygen-rich waters onto coastal TAIs during high tides or storm surges, while groundwater brings more terrestrial-derived organic matter and nutrients to the coastal TAI during heavy rainfall events [*Mopper et al.*, 2015; *Regier et al.*, 2021; *Mattone and Sheaves*, 2017; *Moore*, 2010]. Transport of organic matter and nutrients below and at the surface is then influenced by heterogeneous soil properties and surface morphology, while microbial activity also plays an important role in mediating carbon and nutrient transformations in coastal TAIs [*Lee et al.*, 2006; *Waska et al.*, 2019; *Ganju et al.*, 2019]. In addition, coastal vegetation in wetlands and uplands also shapes hydrological and biogeochemical processes through transpiration and its interactions with soil, water, and microbes [*LaFond-Hudson and Sulman*, 2023; *McDowell et al.*, 2022; *Smith and Kirwan*, 2021; *Zhang et al.*, 2022; *Wang et al.*, 2020; *Krauss et al.*, 2018]. Organic matter of terrestrial origin may provide an additional source of carbon for biogeochemical transformations, while salt marshes may be important carbon sinks [*Xin et al.*, 2022].

Numerical models have been increasingly used to understand the TAI processes [*Fang et al.*, 2022; *Yabusaki et al.*, 2020; *Li et al.*, 2020; *Zhang et al.*, 2022]. However, these models lack an integrated framework that couples surface and subsurface flow and reactive transport processes with ecological processes associated with terrestrial and wetland vegetation for coastal TAI systems. To fill this critical capability gap towards improving our predictive understanding of coupled hydrologic, biogeochemic, and ecological processes in coastal TAIs, we leverage a unique set of mechanistic modeling capabilities that couple the Advanced Terrestrial Simulator (ATS) [*Xu et al.*, 2019] and PFLOTRAN [*Hammond et al.*, 2014] using the Alquimia [*Andre et al.*, 2013] interface. This modeling capability allows us to explore how precipitation, evaportranspiration, and tidal flooding control the exchange fluxes and dynamic biogeochemical transformations at the coastal TAIs. To this end, we specifically selected a 2-D transect that spans a typical open water to upland gradient at a coastal field site in the Chesapeake Bay. By leveraging high-performance computing resources, we explored various simulation scenarios to parse the effects of individual controlling factors on exchanges fluxes and nutrient cycling. Through comparative analysis of different hydrological scenarios, including rainfall and tidal flooding, we observed distinct effects on the oxidation zone with variations in intensity and directional influence. Furthermore, the processes of canopy ET and the presence of decomposed organic carbon were found to introduce additional alterations in reaction conditions and processes within the coastal TAI. Our investigation into the variation of reaction rate constants revealed significant differences, highlighting their influence on redox conditions and the overall system state dynamics. It is important to note that the

model simulations presented here are exploratory in nature and not intended for direct comparisons against field measurements for calibration or validation, the target of a future study.

2 Material and Methods

An integrated modeling approach and experimental data were used in this study. Multiple scenarios based on collected data and reaction parameters estimated from laboratory experiments (Table 2) were employed to study physical and biogeochemical interactions occurring within the soil-water-vegetation system using the ATS model [*Coon et al.*, 2016] and PFLOTRAN reaction sandbox [*Hammond et al.*, 2014; *Hammond*, 2022]. The simulations conducted in this study provided valuable insights into the spatial variability of biogeochemical processes across the coastal interface and allowed us to examine the sensitivity of the ecosystem to different variables, as detailed in Table 3. Through our model, we were able to probe the system's response to various factors and gain a deeper understanding of the complex interactions governing exchange fluxes and redox conditions. The model served as an exploratory tool, enabling us to explore the system's behavior and uncover important patterns and trends.

2.1 Site Description

The study area spans a coastal upland forest, transition region, and brackish wetland near the Chesapeake Bay in Maryland State, USA (Subfigure a in Figure 1). The field team assigned several groundwater sampling points (GW1-GW8) across the study site and installed several groundwater wells at the assigned locations with in-situ aquatic and soil sensors (Subfigure b in Figure 1). To investigate the influence of different processes on carbon, nutrient, and oxygen cycling within the coastal ecosystem, spatially and temporally diverse types of data were collected at the coastal TAI. Field data, including groundwater levels, soil properties (such as moisture and temperature), and carbon concentrations, were collected at each sampling site. A more detailed description of the collected data can be found here (`https://compass.pnnl.gov/FME/DataPublications`).

2.2 Numerical Model Configuration

To numerically investigate the combined effects of multiple processes on carbon cycling and fluxes at the coastal TAI, we constructed a 2-D transect along the GW2 to GW8 flow path. The transect encompasses different land types, including upland, transition, wetland, and open water areas. A diagram of this domain and the distributed plant types are shown in Figure 1 (subfigures b, and c). The present study utilized the ATS Watershed Workflow [*Coon and Shuai*, 2022] to generate the geometry of the transect and meshes of the surface and subsurface domain. The domain spans 215-m horizontally and 18-m vertically with heterogeneous soil properties (Subfigure c in Figure 1). A minimum grid size of 0.05-m was set for the meshing process. The resulting meshes were integrated with spatial data on soil texture, bedrock, and structural characteristics. These data were used to inform the modeling of various hydrological and biogeochemical processes across the transect, contributing to a better predictive understanding of the functioning and dynamics of the studied ecosystem. Additional computational details, including the generation of the meshes, a snapshot of solute concentration in the domain, and the computing environment and demand, are presented in the Supplementary Information.

2.2.1 Flow, Transport, and Water Balance in ATS

ATS is a recently developed multiphysics integrated hydrological simulator [*Coon et al.*, 2016]. It is capable of simulating both surface and subsurface hydrological processes, as well as the exchange of flow between these two domains. Additionally, due to

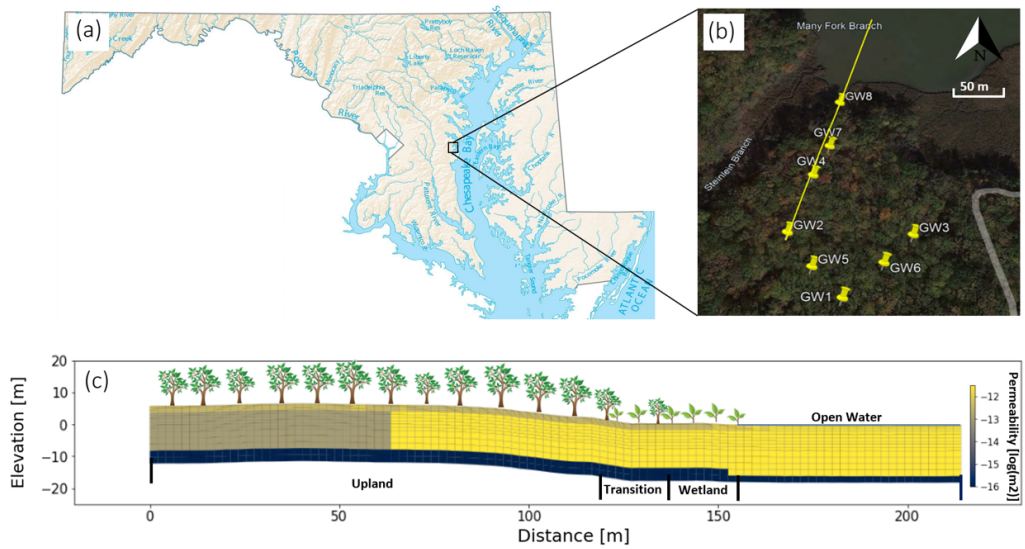

Figure 1: The location map, sampling sites, and conceptual model. (a) Sketch of the river within Maryland and the Chesapeake Bay. (b) The location of the sampling sites where field data, water level, and solute concentration were measured and collected. (c) The permeability field and vegetation types along the selected 2-D transect. The whole domain was separated into four regions, upland, transition region, wetland, and open water, based on plant types.

the flexible design of the Process Kernels (PKs) tree, ATS can simulate the presence or absence of vegetation and associated processes. This feature enables the examination of how vegetation influences solute transport dynamics and the role of vegetation in solute transport. ATS solves the Richards equation for the subsurface domain coupled to the surface flow equation including the source terms, sink terms, and ET. The ET processes, including canopy interception, transpiration, and bare ground evaporation, are implemented using a one-layer radiation balance and Priestley-Taylor model for potential evaporation, as described in [*Coon et al.*, 2016] and [*Oleson et al.*, 2013]. Information about the governing equations can be found in the Supplementary Information.

2.2.2 Biogeochemical Function in PFLOTRAN

We employed a simplified biogeochemical reaction network, which includes aerobic respiration and two-step denitrification, to simulate carbon and oxygen dynamics and nitrogen transformations. Dissolved organic carbon (CH_2O) is oxidized to CO_2 by three electron acceptors (i.e., O_2, NO_3^-, and NO_2^-):

$$\text{Aerobic respiration (AR)}: CH_2O + O_2 \rightarrow CO_2 + H_2O \tag{1}$$

$$\text{Denitrification (DN 1)}: CH_2O + 2NO_3^- \rightarrow CO_2 + 2NO_2^- + H_2O \tag{2}$$

$$\text{Denitrification (DN 2)}: CH_2O + 4/3NO_2^- + 4/3H^+ \rightarrow CO_2 + 2/3N_2 + 5/3H_2O \tag{3}$$

The reaction rates follow Michaelis–Menten kinetics with a regulating term. The unregulated reaction rate ${R_i}^{kin}$ has the form of

$${R_i}^{kin} = V_{max} \left(\frac{C_i^D}{K_i^D + C_i^D} \right) \left(\frac{C_i^A}{K_i^A + C_i^A} \right), \; i = 1, 2, 3 \tag{4}$$

where V_i^{max} is the maximum reaction rate (in $1/d$) and C_i^D and C_i^A are the concentrations of the electron donors and acceptors, respectively. K_i^D and K_i^A are the half-saturation constants for the electron donors and acceptors, respectively. K_i^D is set at 0.25 mM for all three reactions [*Zheng and Doskey*, 2015]. K_i^A is set at 0.001 mM, 0.001 mM, and 0.004 mM for AR, DN 1, and DN 2, respectively [*Song et al.*, 2018].

The regulation term follows the cybernetic control law, where the cybernetic variable ${e_i}^{rel}$ represents the relative enzyme level for a given reaction. Here we adopted *Song et al.* [2018] and *Song and Ramkrishna* [2011] to determine ${e_i}^{rel}$ using the simplified formulation:

$$ {e_i}^{rel} = \frac{{R_i}^{kin}}{\sum_{j=1}^{3} {R_j}^{kin}},\ j = 1, 2, 3 \tag{5} $$

The regulated reaction rate is the product of the cybernetic variable and the unregulated reaction rate:

$$ R_i = {R_i}^{kin} {e_i}^{rel},\ i = 1, 2, 3 \tag{6} $$

The above reactions and kinetic expressions are implemented into the PFLOTRAN reaction sandbox [*Song et al.*, 2018]

2.2.3 Boundary and Initial Conditions Based on Field Data

We assigned Dirichlet conditions as hydrological boundary conditions at the uphill (left) and seawater (right) sides for both the surface and subsurface domains, based on observed water levels. In particular, GW2 water levels collected from the field were used as the left uphill boundary. Tide level data for the coastal region were acquired from the United States Geological Survey tide gauge located at Chesapeake City, MD (site ID: 8573927). The data source can be accessed online (`https://tidesandcurrents.noaa.gov/waterlevels.html?id=8573927`). Precipitation data were assigned to the surface top using the Daymet data shown in Figure 2. It is also important to note that no flow boundary condition was applied to the bottom of the subsurface domain due to the presence of impermeable rocks in that region. Solute boundary conditions were collected from in-situ concentration data from the Coastal Observations, Mechanisms, and Predictions Across Systems and Scales (COMPASS) project, a long-term database of Global Change Research wetlands (`https://serc.si.edu/gcrew`), and the values in articles [*Song et al.*, 2018; *Nelson et al.*, 2017; *Menendez et al.*, 2022; *Spalding and Exner*, 1993; *Rich et al.*, 2008]. Based on the setup in Table 1, groundwater provided the largest concentration of DOC and NO_3, while higher O_2 comes from surface water.

Table 1: Concentrations of boundary conditions for various species.

Solute	Rainwater	Groundwater	Surface Seawater	Subsurface Seawater
$CH_2O\ (MgC/L)$	1.20E-06	1.35E+01	4.18E+00	4.18E+00
$O_2\ (Mg/L)$	3.20E-06	7.00E-02	7.00E-02	7.50E+00
$CO_2\ (Mg/L)$	4.41E-06	3.39E+04	3.52E+02	2.64E+03
$NO_3^-\ (Mg/L)$	6.20E-06	5.00E+00	0.44E-01	0.44E-01
$N_2\ (Mg/L)$	2.80E-06	2.80E-06	2.80E-06	2.80E-06
$NO_2^-\ (Mg/L)$	4.61E-06	4.61E-06	4.61E-06	4.61E-06
$NH_4^+\ (Mg/L)$	1.80E-06	1.06E+00	1.80E-02	1.80E-02
$C_5H_7O_2N\ (Mg/L)$	1.80E-04	1.80E-01	1.80E-01	1.80E-01

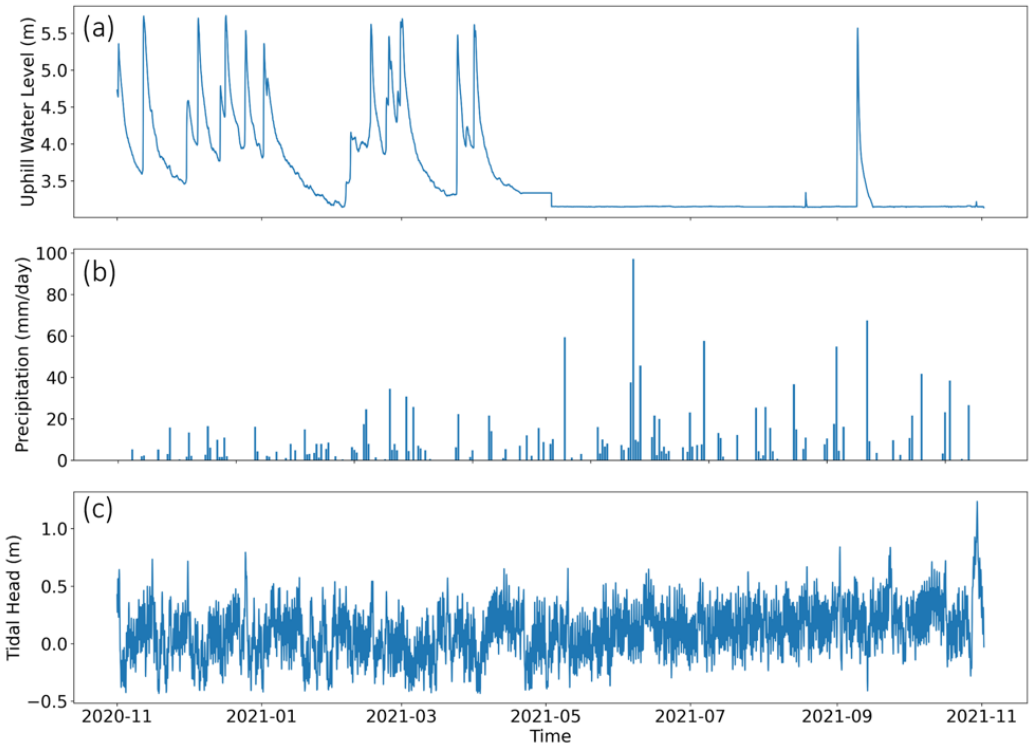

Figure 2: Subfigures illustrating variations in the uphill water level, precipitation, and tide head over the study period. (a) shows the fluctuations in water level at the uphill location (GW2). (b) shows the temporal distribution of precipitation, with the maximum precipitation occurring on day 218. (c) shows tidal head measurements at the specified locations, with the highest tidal head occurring on day 363. These data provide dynamic hydraulic conditions for reactive transport simulations.

To investigate the impact of the aerobic respiration rate on carbon cycling within TAIs, we conducted experiments and utilized AquaMEND to estimate the maximum reaction rate constants V_{max} in Eq.(4) for aerobic respiration on samples obtained from the COMPASS project. The calculated maximum reaction rate values are displayed in Table 2. In the coastal zone, we obtained nine sets of reaction maximum constant values for different regions, with a notable 7.8-fold difference. Additionally, considering the limited availability of data, we used the values reported by *Song et al.* [2018] for other biogeochemical parameters.

Table 2: The calculated reaction rate constant for aerobic respiration.

Upland forest (1/d)	Transitional forest (1/d)	Wetland (1/d)
$V_{max,1}$: 24.84	$V_{max,4}$: 35.20	$V_{max,7}$: 54.16
$V_{max,2}$: 33.44	$V_{max,5}$: 38.80	$V_{max,8}$: 158.08
$V_{max,3}$: 42.22	$V_{max,6}$: 47.66	$V_{max,9}$: 195.47

The determination of vegetation types, forest and grassland, along the 2-D transect was based on combined data from the national land cover database and fieldwork. Based on plant types, additional data such as air temperature, leaf area index, and other relevant information were obtained from the Daymet dataset using Watershed Workflow [*Coon and Shuai*, 2022]. Daymet provides atmospheric forcings with high spatial and temporal resolutions across North America. The purpose of incorporating these boundaries, initial conditions, and observational data into the model is to achieve a comprehensive understanding of how hydrological and ecological processes affect carbon cycling. To accomplish this, the surface and subsurface flow was initially simulated to a dynamic steady state and reactive transport was simulated with appropriate initial and boundary conditions. For more specific information, please refer to the Supplementary Information section of the paper.

2.2.4 Simulation Scenarios

Numerical experiments investigate the influence of environmental factors on redox condition and carbon cycling in coastal TAIs. The study comprises four aspects and a total of 13 scenarios. These aspects focus on the effects of precipitation and tidal changes, canopy evapotranspiration, surface desorbed DOC, aerobic respiration rates on exchange fluxes, redox conditions and carbon cycling, see Table 3.

By comparing scenarios 1, 2, and 3, we investigated the effects of inundation and precipitation on exchange fluxes and oxygen transport. Since high oxygen originates from the surface layer of seawater, changes in fluxes due to variable rainfall and inundation will directly affect oxygen transport. Therefore, we distinguished scenarios 1, 2, and 3 according to their hydraulic conditions. To isolate the dynamic effects of precipitation and inundation on the reactions, we used average values to limit one factors to a constant value while leaving the other dynamic. This approach allows us to test the specific effects of dynamic precipitation and inundation on the redox conditions within the coastal TAI subsurface.

Scenarios 4 and 5 demonstrate two important effects related to vegetation within the coastal TAI ecosystem. In scenario 4, we introduce vegetation-related processes, specifically focused on the impact of ET in vegetated regions. Scenario 5 incorporates an external DOC source term to simulate the decomposition of organic matter from plants over vegetated regions. By comparing these scenarios to the baseline scenario, 1, we can

analyze the individual and combined effects of vegetation and external DOC on the carbon cycling and overall ecosystem dynamics within the coastal TAI. This comparison enables a comprehensive assessment of how vegetation-related processes and external DOC inputs influence the carbon cycling and ecological functioning of the studied ecosystem.

We compared scenario 6 to scenario 13 and scenario 1 to investigate the influence of reaction conditions on carbon cycling within the coastal TAI. These scenarios have a modified reaction rate constant for aerobic respiration, representing different reaction conditions at various site positions within the TAI. Each scenario is associated with a specific reaction rate constant ($V_{max,1}$ to $V_{max,9}$). This comparison allows us to examine how variation in reaction rate constants affects carbon cycling dynamics. By altering the reaction conditions at different site positions within the TAI, we can assess the impact of these variations on carbon cycling processes. The results provide valuable insights into the biogeochemical processes underlying carbon cycling and their associations with different environmental factors.

Table 3: Scenarios with different hydrological, ecological, and reaction conditions.

Scenario	Variable Rainfall	Variable Tide	Canopy ET	Desorbed DOC	Rate Constant
1	Yes	Yes	No	No	$V_{max,1}$
2	Yes	No	No	No	$V_{max,1}$
3	No	Yes	No	No	$V_{max,1}$
4	Yes	Yes	Yes	No	$V_{max,1}$
5	Yes	Yes	No	Yes	$V_{max,1}$
6	Yes	Yes	No	No	$V_{max,2}$
7	Yes	Yes	No	No	$V_{max,3}$
8	Yes	Yes	No	No	$V_{max,4}$
9	Yes	Yes	No	No	$V_{max,5}$
10	Yes	Yes	No	No	$V_{max,6}$
11	Yes	Yes	No	No	$V_{max,7}$
12	Yes	Yes	No	No	$V_{max,8}$
13	Yes	Yes	No	No	$V_{max,9}$

3 Results and Discussion

3.1 Exchange Fluxes at the TAI Driven by Precipitation, Tidal Change, and Evapotranspiration

By comparing three scenarios (scenarios 1 to 3), we investigate the effects of precipitation and flooding on exchange flux across coastal ecosystems. The baseline scenario (scenario 1) shows that varying precipitation and tide change result in dynamic exchange flux across the whole 2-D transect that vary across both space and time (Figure 3).

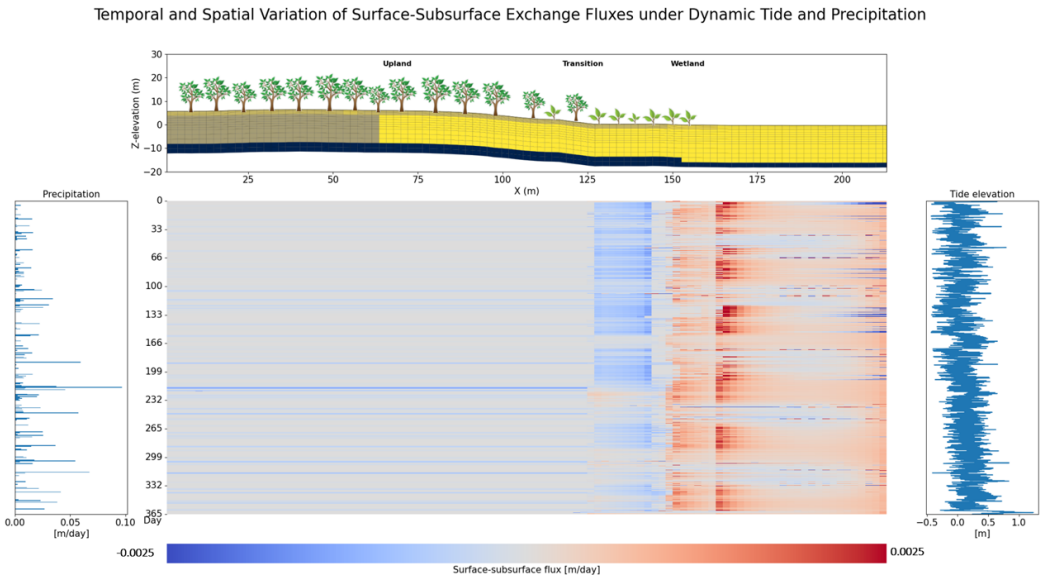

Figure 3: This figure presents the spatiotemporal dynamics of the flow exchange flux between the surface and subsurface domains, influenced by dynamic precipitation and tidal changes. The top subplot visualizes the distribution of vegetation along a 2-D transect, accompanied by the corresponding transect elevation. The left and right subplots display temporal variations in precipitation and tidal elevation from November 2020 to November 2021. The middle subplot depicts the hourly exchange fluxes between the surface and subsurface domains. The variations in flux magnitude and direction are represented through color gradients, with warmer colors indicating stronger upwelling fluxes.

In the presence of rainfall, the uphill side experiences dominant downwelling fluxes with strong precipitation contributing to an amplified flux increase. For example, an apparent heavy rain [*Bhatla et al.*, 2019] event occurred on day 218, triggering the most powerful downwelling flux from the surface to the subsurface domain. The upwelling flux is primarily distributed along the open water side. The movement of groundwater from inland areas towards the coast can result in the upwelling of groundwater with DOC and nitrate near the shoreline. For a comprehensive exploration of the flow path and tracer test results, please refer to the Supplementary Information. A larger upwelling flux occurs when the sea water level is lower. Notably, the transition and wetland regions, characterized by frequent interactions between terrestrial and aquatic environments, exhibit a distinct hot exchange flux hotspot. To be specific, the inundation process causes the difference in the downwelling flux between the transition and upland. Variations in tide height alter the strength and position of the downwelling flux at the coastal TAI. Consequently, diverse hydrological conditions can lead to a directional change in fluxes. Dynamic tidal levels and precipitation affect the intensity of exchange fluxes, especially from

the transition to wetland regions. To further analyze the individual effects of dynamic precipitation and tide change, the exchange flux across the 2-D transect of scenarios 2 and 3 have been analyzed and are shown in the Supplementary Information.

Furthermore, canopy ET influences the water balance within the TAI. Scenario 4 was conducted to investigate the effect of vegetation after considering the related ET process. Based on the national land cover database and field pictures, we identified two main types of plants along the 2-D transect: deciduous forest and grassland. In scenario 4, the canopy information and relative LAI, humidity, temperature, shortwave radiation, evaporation, and transpiration processes were assigned to the whole domain. Figure 4 shows the difference in exchange flux after considering the vegetation and related ecological processes.

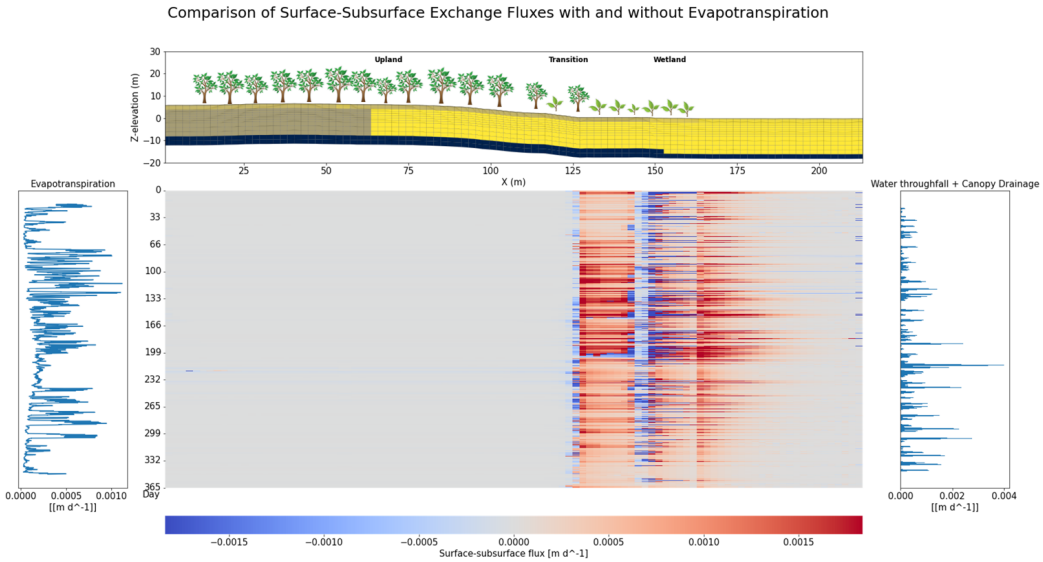

Figure 4: Alterations in flow exchange fluxes resulting from vegetation-related ecological processes over a one-year period, from November 2020 to November 2021. The subplot on the left depicts ET, the right subplot shows the water throughfall and canopy drainage across a 2-D transect. The middle subplot portrays the changes in hourly exchange fluxes between the surface and subsurface domains when accounting for the vegetation-related ecological processes. The results indicate that the exchange fluxes in the transition and wetland areas are particularly sensitive to these processes. Additionally, the upwelling flux is amplified when ET is strong, especially during the summer season.

The most substantial hydrological differences were observed from the transition to wetland regions, since the uphill soil layer maintains unsaturated conditions for long time periods (shown in Figure 5). Comparing the ET, canopy drainage, and water throughfall in Figure 4, the main difference of exchange flux happened with higher ET values. Strong exfiltration processes will bring more water from the subsurface to the surface and enhance the upwelling fluxes. Intense canopy drainage and water throughfall enhance the downwelling flux. Therefore, temporal variations in dynamic exchange flux differences emerged as a result of transpiration and evaporation processes across the entire domain. To further quantify the temporal effect of vegetation on exchange flux within the TAI, we calculated the averaged exchange flux along the TAI for different seasons, shown in the Supplementary Information. The most prominent distinction of exchange flux arises during the summer season, which can be attributed to the elevated temper-

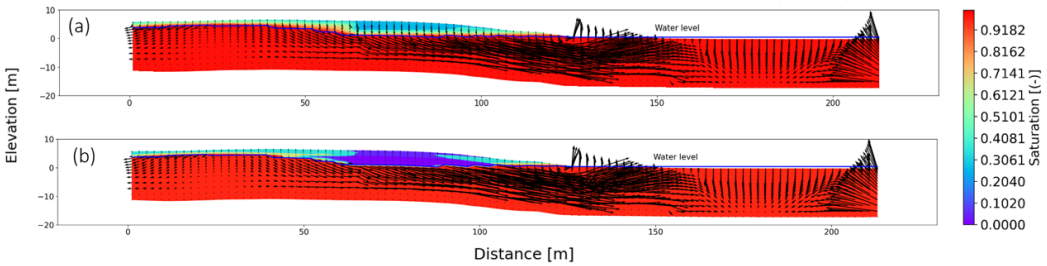

Figure 5: Saturation, flow paths, and water level comparisons between cases with and without vegetation. (a) and (b) depict scenarios 1 and 4, respectively, on day 218.

atures and increased ET rate experienced during this period. Hence, the presence or absence of vegetation exerts a notable influence on the exchange flux. In vegetated regions, soil saturation can decrease by over 20%, leading to alterations in the local solute concentration (shown in Figure 5).

3.2 Precipitation and Tide Change: Dispersion and Concentration of Oxygen in the TAI Subsurface Domain

The transition and wetland regions, where there is frequent interaction between terrestrial and aquatic environments, give rise to the formation of a hot spot for exchange fluxes. Variations of exchange flux within the TAI are tightly connected with the underlying redox condition. For example, during floods, a larger quantity of oxygen will be transported from the seawater towards the transition zone. This leads to the creation of a region with high oxygen concentration below the transition zone where downwelling flow occurs. Meanwhile, the lower oxygen infiltrated water will also transport from upland to the mixing zone. We observed that most of the downwelling oxygen fluxes occured in the transition zone and certain parts of the wetland (Figure 6). As a result, the specific location of the transition point, where the oxygen-rich (oxic) zone transitions to the anoxic (hypoxic) zone, varies in response to the dynamic water levels shown in Figure 7.

To investigate the individual effects of dynamic precipitation and tide change on the redox condition within the TAI, two scenarios (2 and 3) were simulated, each focusing on a single dynamic variable. The temporal vertical distribution of oxygen at the transition (125 m) and wetland (150 m) locations was then analyzed for each scenario, depicted in Figure 8. This analysis provides insights into the impact of these dynamic variables on the oxygen levels at specific locations within the system.

From scenario 2, we observed both distinct similarities and differences in the redox conditions between the transition and wetland regions in response to varying precipitation patterns. In the transition region, the oxygen-rich zone is primarily located near the soil surface. In the wetland region, the oxidation zone is both larger and deeper. This distinction can be attributed to the constant tidal constraint, which impedes the transport of oxygen-rich water to the transition region during flood events. Moreover, both areas are influenced by dynamic precipitation, which impacts the oxygen concentration levels. Infiltration brings freshwater from upland areas into the wetland region, thereby influencing the horizontal and vertical distribution of the coastal TAI subsurface. Although the wetland areas exhibit greater resistance to dilution, both the transition and wet regions experience a decrease in oxygen concentration during periods of precipitation. The heavy rainfall event on day 218 caused a significant dispersion of oxy-

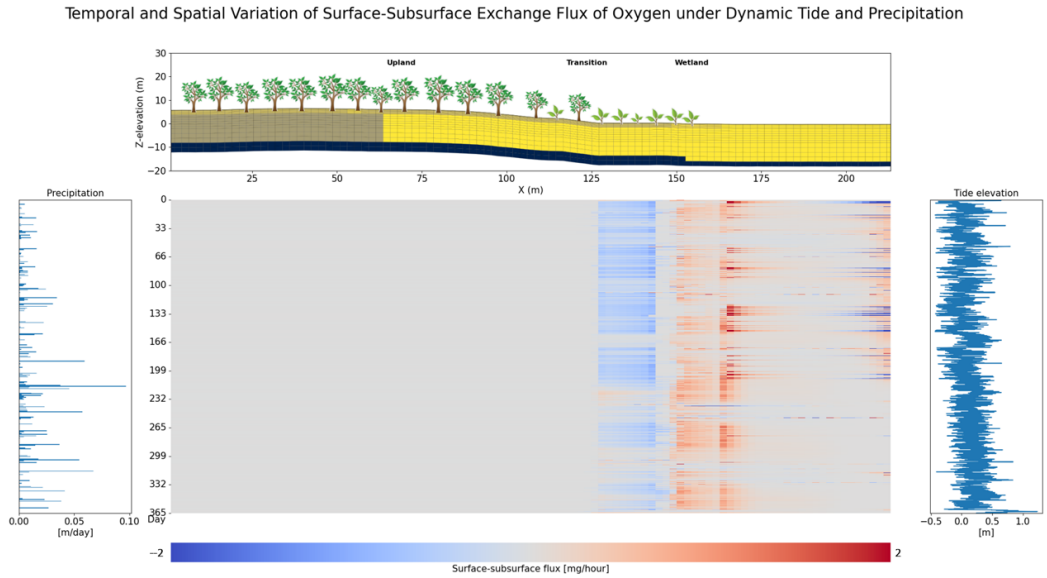

Figure 6: The oxygen exchange flux between the surface and subsurface domains varies with dynamic precipitation and tidal changes. The middle subplot shows the hourly oxygen exchange fluxes between the surface and subsurface domains.

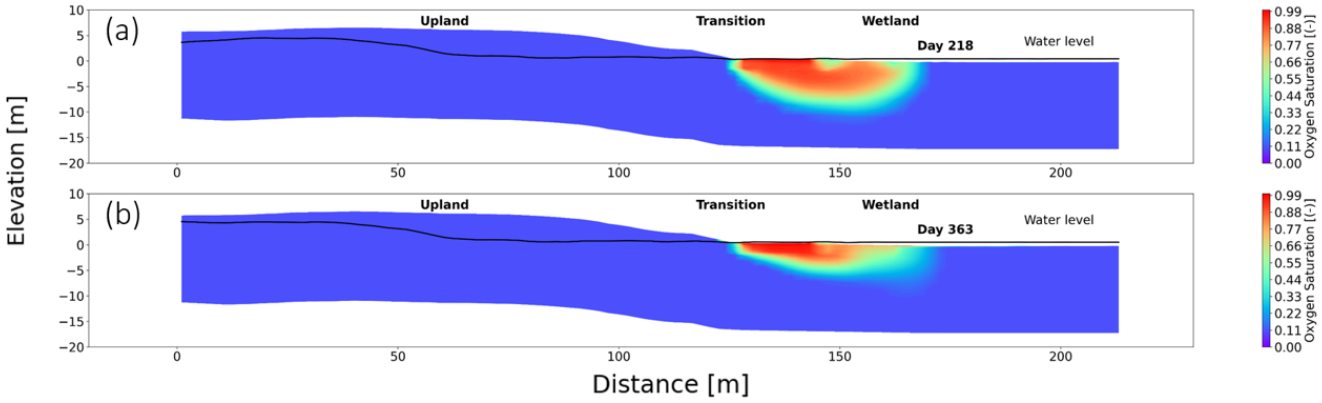

Figure 7: These sub-figures depict the oxygen concentration distribution during two extreme weather events: the largest precipitation event and the strongest inundation event. The precipitation and tide data were collected from NOAA's station and Daymet near the study area. The results are presented as color-coded maps. The warmer colors indicate higher oxygen concentrations, while the cooler colors represent lower concentrations. The figures provide insight into the impact of extreme weather events on oxygen availability in terrestrial aquatic ecosystems, which is crucial for redox reaction process. The comparison between the two sub-figures highlights how the two events affect oxygen concentration levels differently.

gen concentrations in the wetland area, resulting in noticeable declines both vertically and longitudinally.

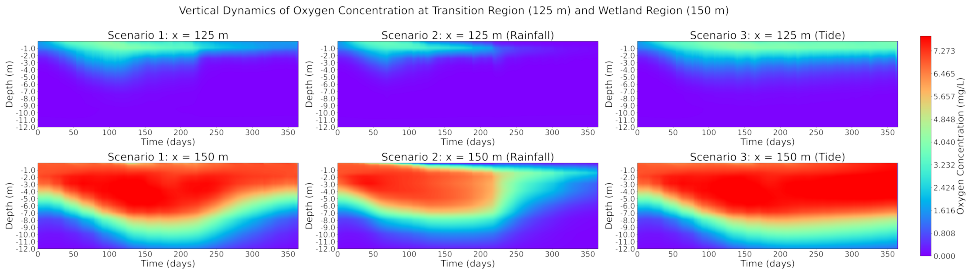

Figure 8: Heatmaps depicting the spatiotemporal variations in oxygen concentration across different scenarios and locations over a one-year period. The figure consists of three columns, each representing a specific scenario: dynamic tide and varying precipitation (column 1), dynamic precipitation (column 2), and dynamic tide (column 3). Each column is further divided into two rows, with the top row corresponding to the transition region (x = 125m) and the bottom row representing the wetland region (x = 150m). The color-coded heatmaps visualize the changes in oxygen concentration, providing valuable insights into the seasonal and spatial dynamics of oxygen levels within the study area.

The results of scenario 3 show the influence of flooding caused by high tide levels, which facilitates the inflow of oxygen into the transition region through horizontal overland flow. In contrast to the lower oxygen concentrations observed in the top soil location of scenario 2, scenario 3 demonstrates that dynamic tidal changes, particularly during strong flooding events, lead to an increased inward flow of oxygenated seawater. As a result, a larger oxidation zone is formed, with the transition zone experiencing a more significant rise in oxygen levels vertically. Both the transition and wetland zones exhibit higher oxygen concentrations compared to scenario 2. The absence of dynamic rainfall effects allows the high oxygen state maintained by dynamic tides at greater depths to extend even further. To summarize, scenario 3 reveals that the interaction between dynamic tidal changes and flooding enables the transportation of oxygenated seawater, leading to higher oxygen concentrations and an expanded oxidation zone in both the transition and wetland zones.

Through our research, we have observed that strong inundation has a dual impact on the hydrological processes and solute transport. First, it raises the water level, allowing solutes from seawater to enter the transition zone. Second, it expands the mixing zone for solute transport in both the vertical and horizontal directions. Surface runoff caused by precipitation and groundwater promotes the dispersion of solutes in the upper and deeper layers of the soil, respectively. These hydrological processes play a significant role in shaping redox conditions, particularly during heavy rainfall and flooding events.

3.3 Evapotranspiration and External Carbon Sources: Impacts on Water Availability and Solute Concentration in Ecosystems

In this section, we conducted a more in-depth analysis of the alterations in reactants within the reaction network, taking into account the influences of ET and exter-

nal carbon sources. The first column in Figure 9 shows the original distribution of oxygen, DOC, and nitrate in scenario 1. As expected, the oxygen concentration is higher at the uppermost part of the subsurface domain. Simultaneously, the groundwater transported a greater amount of DOC and nitrate from uphill areas to the TAI, leading to elevated levels of DOC and nitrate in the lower region. Moreover, the variation of water balance also affects the solute concentration. In particular, the evaporation process will decrease the saturation of soil and increase the solute concentration, shown in Figure 5. As a result, elevated concentrations of reactants were observed in upland and transition areas, attributed to the concentration effect caused by evaporation process. The concentration effect influences the local concentration and causes an increase in the oxygen content, especially in the case shown in Figure 9. The third column in Figure 9 shows the disparities in carbon, nitrate, and oxygen in the presence or absence of ET. The figure illustrates the variations in these components and highlights the impact of ET on their dynamics. As a result of ET processes, the concentrations of oxygen and DOC in the surface and topsoil layers of the subsurface increase. The accumulation of oxygen in these areas leads to a modification of the redox conditions in the TAI subsurface region. The shift towards more oxidizing conditions facilitates the consumption of DOC, intensifying oxidation reactions. Consequently, the increased rate of oxidation reactions regulates the nitrification process, resulting in higher nitrate levels in deeper soil layers.

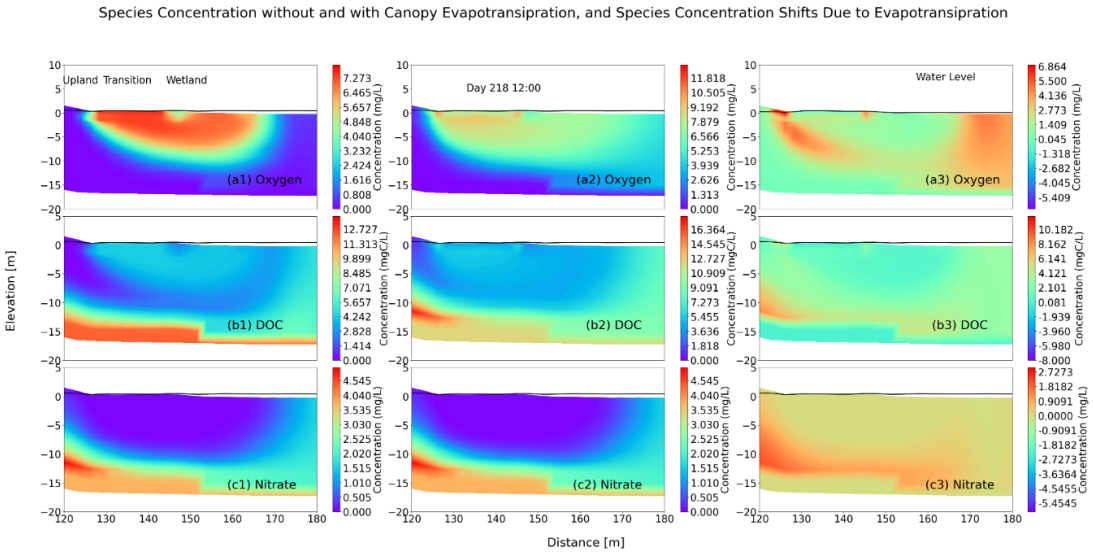

Figure 9: Comparison of oxygen, DOC, and nitrate concentrations in two scenarios (1 and 4) in three columns. The first column represents species concentrations without considering canopy ET, the second column represents concentrations when canopy ET is considered, and the third column illustrates the change in species concentration due to the consideration of canopy ET. The top row displays oxygen concentrations, the middle row shows DOC concentrations, and the bottom row represents nitrate concentrations. The contour maps visually represent the spatial patterns and relative changes in species concentrations, providing insights into the impact of canopy ET on the dynamics of oxygen, DOC, and nitrate.

Other than the indirect effect of increasing concentration via evaporating water, the decomposition process of vegetation affects the redox reaction process more directly by creating an external DOC source. In scenario 5, we assigned the external DOC source term to the vegetated region along the 2-D transect to analyze its effects on carbon cycling. The DOC concentration was estimated based on the relationship between DOC

concentration and precipitation, equation 7 [*Oh and Choi*, 2022]. To be specific, we allocated the concentration of DOC, denoted as y and measured in MgC/L, to the precipitation variable, denoted as x and measured in mm/d. This assignment was made to simulate the decomposition processes associated with rainfall in our research. By doing that, a varying DOC source dependent on precipitation will be added to mimic the decomposed DOC (see the figure in Supplementary Information). To analyze the influence of external DOC sources on carbon cycling at the TAI, we compared the species concentration in scenario 1 and scenario 5. The variation of oxygen, carbon, and nitrate is shown in Figure 10.

$$y = 0.049 * x + 1.801 \tag{7}$$

The dynamics of precipitation and related external DOC contribute to the heterogeneity of DOC distribution. Surface runoff can drive DOC-rich water from upland to wetland regions on the surface. Within the TAI, A clear increase of DOC occurred in the downwelling zone and was transported along the flow path within the subsurface (Figure 10). The increase of DOC led to more consumed oxygen along the flow path due to the increase in reaction rate. Therefore, the oxygen concentration differs along a flow path with more DOC. Meanwhile, the nitrate is also affected in the deep zone as DOC is transported into the deeper zone. This increases the denitrification reaction rate, leading to the conumption of more nitrate.

Our results indicate that the addition of external carbon sources leads to an increase in carbon concentration and alters the carbon cycling, nitrogen cycling, and oxygen consumption rates. These impacts are not equally distributed along the coastal TAIs subsurface. Our findings are consistent with the study of *McClain et al.* [2003] on the dependence of reaction conditions on flow paths. Similar to their study, we observed that the quality of transport to a given region had a significant impact on the observed results. The consistency further emphasizes the importance of managing external carbon sources in ecosystem management practice.

In this section, we analyzed the ecological influence of vegetation on exchange fluxes and reaction conditions in the TAI. Results showed that transition and wetland areas were particularly sensitive to these processes, with amplified upwelling fluxes during strong ET. The concentrated reactants and addition of external carbon sources affected carbon and nitrogen cycling, oxygen consumption rates, and carbon concentration with non-uniform distribution in coastal TAIs. Therefore, considering vegetation and related products is crucial for optimizing ecological outcomes. After analyzing hydrological processes, particularly events, the next section involves investigating the impact of reaction rates on carbon cycling, taking into account the influence of significant hydrological events.

3.4 The Impact of Aerobic Respiration Rate on Carbon Cycling in Ecosystems

Sampling from different regions of the coastal TAI shows that reaction conditions substantially vary from upland to transition to wetland, shown in Table 1. To further investigate the sensitivity of carbon cycling to redox reaction rate in these regions, we conducted a series of simulations assuming different estimated reaction rate constants for distinct zones of the TAI. From scenario 6 to 13, a constant aerobic respiration rate constant was adopted for the entire 2-D model domain. Our analyses focus on the subregion between 120 meters and 180 meters, which was identified as the most active area for exchange fluxes and redox transformations. By focusing on this specific range, we quantified the effect of key factors on the dynamic behavior of the oxic zone in the TAI. Based on previous studies, we compared the sensitivity of carbon cycling to aerobic respiration rates under two distinct hydrological events: heavy rain (occurring on day 218) and strong

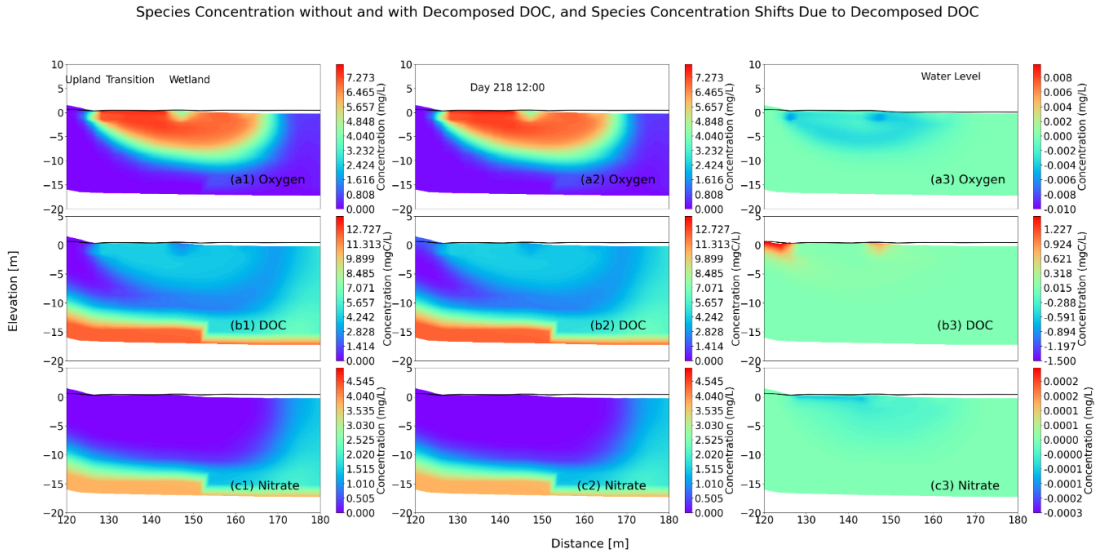

Figure 10: Comparison of oxygen, DOC, and nitrate concentrations for two scenarios (1 and 5) in three columns. The first column represents species concentrations without considering decomposed DOC, the second column represents concentrations when decomposed DOC is included, and the third column illustrates the change in species concentration resulting from the inclusion of decomposed DOC. The top row displays oxygen concentrations, the middle row shows DOC concentrations, and the bottom row represents nitrate concentrations. The contour maps visually depict the spatial patterns and relative changes in species concentrations, providing insights into the impact of decomposed DOC on the dynamics of oxygen, DOC, and nitrate.

flooding (occurring on day 363). We examined the difference in carbon cycling between fast and slow reaction rate cases for both events. Figure 11 for day 218 illustrates the oxygen, DOC, and nitrate distribution during the heavy rain event, while the Figure 12 for day 363 represents the oxygen, DOC, and nitrate distribution during the strong inundation event. By comparing the response of reactive species concentrations between these events, we can understand how aerobic respiration rates affect the carbon cycle of different hydrological events in coastal TAIs.

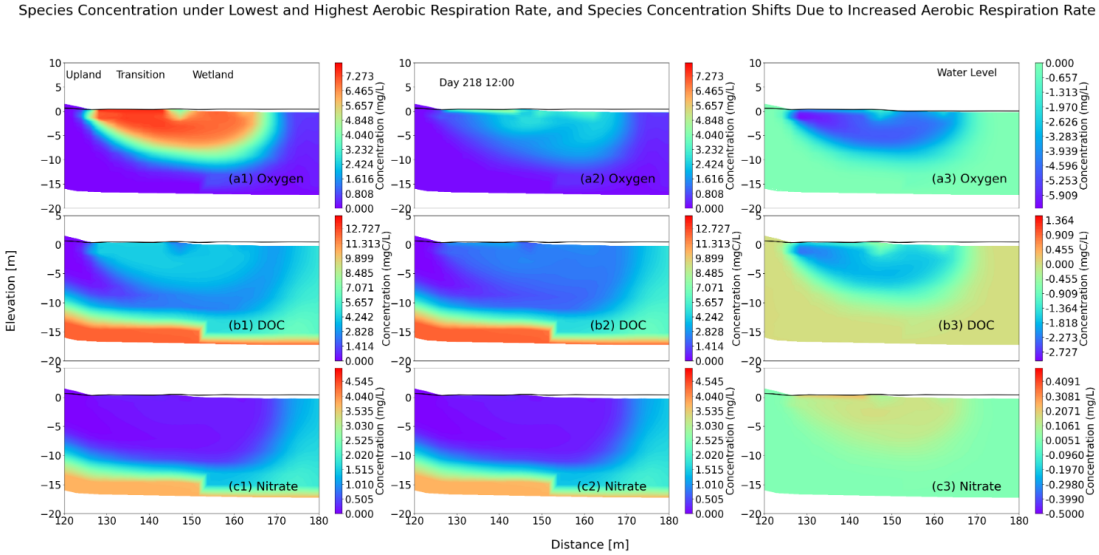

Figure 11: Comparison of species concentrations during a heavy rain event on day 218, focusing on aerobic respiration rates. The graph consists of three columns. The first column represents species concentrations associated with the lowest aerobic respiration rate. The second column represents species concentrations associated with the highest aerobic respiration rate. The third column illustrates the shifts in species concentrations resulting from the increase in aerobic respiration rate. The species analyzed include oxygen, DOC, and nitrate, highlighting the impact of aerobic respiration rates on oxygen, DOC, and nitrate dynamics.

Significant differences in carbon, nitrate, and oxygen were found between the highest and lowest aerobic rate cases shown in Figure 11. The higher rate of aerobic respiration consumed more oxygen and DOC within the oxic zone. The largest difference occurs in regions of high oxygen content, because the oxygen level is the reaction limiting at the higher consumption rate. The amount of oxygen in the surface soil of the transition zone is not sufficient for the more active redox reaction processes and will be consumed to the maximum extent. Thus, the largest difference is seen in higher oxygen locations. Correspondingly, DOC are involved in this process as electron donors, resulting in a similar difference pattern as seen in the higher rate conditions. There is a minor difference of DOC within the deeper zone compared to the difference in oxygen concentration in the topsoil, which resulted from denitrification processes. The nitrate differences figure shows that the nitrate us higher under a more active aerobic respiration rate case. Regulation of the reaction rate, as described in the equation 6, is responsible for this phenomenon. When the rate of aerobic respiration increases, the regulatory effect decelerates the denitrification process. As a result, large amounts of nitrate accumulate in the deeper anoxic soil regions. During intense flooding events, such as in Figure 12, there are notable changes in the location of areas where deficits occur and in the absolute differences of oxygen, DOC, and nitrate levels. These changes can be attributed

to the solute composition of rainfall, groundwater, and seawater. The occurrence of a strong flooding event led to an influx of additional oxygen in both cases, resulting in a reduction of the oxygen difference caused by variations in oxidation reactions. The difference in DOC consumption between fast and slow reactions was mitigated in the high oxygen condition, and therefore, DOC consumption reduced the difference in DOC on the TAI surface soil.

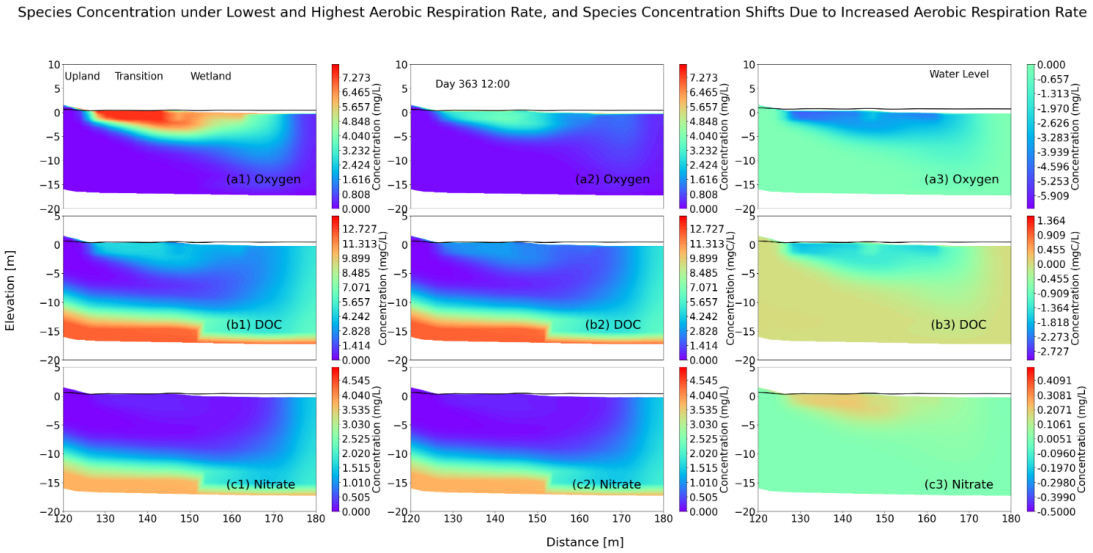

Figure 12: The spatial distribution of key reactants, such as oxygen, DOC, and nitrate, during a significant flooding event on day 363. The results illustrate reactant concentrations associated with both the lowest and highest aerobic respiration rates. The figure shows the differences in species concentration between the highest and lowest aerobic respiration rates observed during the strong flooding event on day 363.

The difference between high and low rate cases indicates that the reaction rates have a significant influence on reaction processes and solute distribution. To assess the impact of reaction rates on environmental conditions, we performed calculations to quantify the proportion of oxic, hypoxic, and anoxic zones within the selected TAI. By employing defined thresholds of 2 Mg/L for hypoxic and 0.2 Mg/L for anoxic [*Menendez et al.*, 2022], we computed the respective areas of by the oxic, hypoxic, and anoxic zones. The variations in the fraction of these zones for nine different rate conditions are illustrated in Figure 7.

The fraction of the oxic, hypoxic, and anoxic zones dynamically changed throughout the year, primarily influenced by precipitation and tidal variations. In general, the lower reaction rate sustained a high proportion (20%-40%) of the oxic zone and the higher reaction rate case resulted in more anoxic conditions, with an anoxic zone fraction value from 45% to 62.5%. As discussed in previous sections, precipitation affects the redox condition in both the vertical and horizontal directions and enlarges the redox zone. During periods of heavy rainfall, the fraction of the oxic zone tends to increase, resulting in a reduction in the proportion of the anoxic zone. Therefore, we see the peak of the oxic zone when heavy rain occurs. However, the overall relationship between these zones also depends on the reaction rates, especially in cases where the aerobic respiration rate is relatively high. With high respiration rates, the accumulated oxygen will be continuously consumed as the reaction proceeds. This will lead to a deficiency of oxygen at higher rate conditions. Therefore, the fraction of oxic zone shows a tendency to increase and then

decrease. The fraction of the oxidation zone in the high rate case decreases earlier than in the slow rate case (scenario 12 and scenario 13). This decrease was sustained even when a heavy rain event occurred during this process. This is because the dilution effect of heavy rainfall in this low oxygen concentration case turns the oxic zone into a hypoxic zone or even an anoxic zone. In contrast, the anoxic area showed an opposite trend to the oxic area with the effect of rainfall and tidal changes. In all cases, the lowest fraction of anoxic zone occurred during the occurrence of Harvey rain. Remarkably, we observe a more stable hypoxic zone. The variation of its area is only 10% of the total area even for different reaction rates, compared to about 20% for the oxic and anoxic zones. As an intermediate region between the oxic and anoxic zones, it can be transformed into two external regions with the dynamic process of hydrology, while also giving rise to more complex dynamics. For example the two cases at high reaction rates show different trends than the other seven cases. This depends mainly on the fact that faster reaction rates consume more oxygen, causing the original balance between chemical reaction consumption and oxygen transport replenishment to change and become more sensitive.

Our results have shown that carbon storage in ecosystems decreases when the rate of aerobic respiration increases, while a decrease in the rate of respiration leads to an increase in carbon storage. These findings highlight the critical role of aerobic respiration in the rate of carbon cycling and its impact on the overall carbon balance of ecosystems. Furthermore, oxygen levels in TAI can be used as a measure of the rate of aerobic respiration.By comparing the variation of redox components among three different groups, i.e., uplands, transition zones and wetlands, it is clear that redox conditions exhibit greater dynamics in wetlands (Figure 13). A wider range of variation in wetland reaction rates would lead to more dynamic changes in redox conditions and would have more important implications for carbon storage.

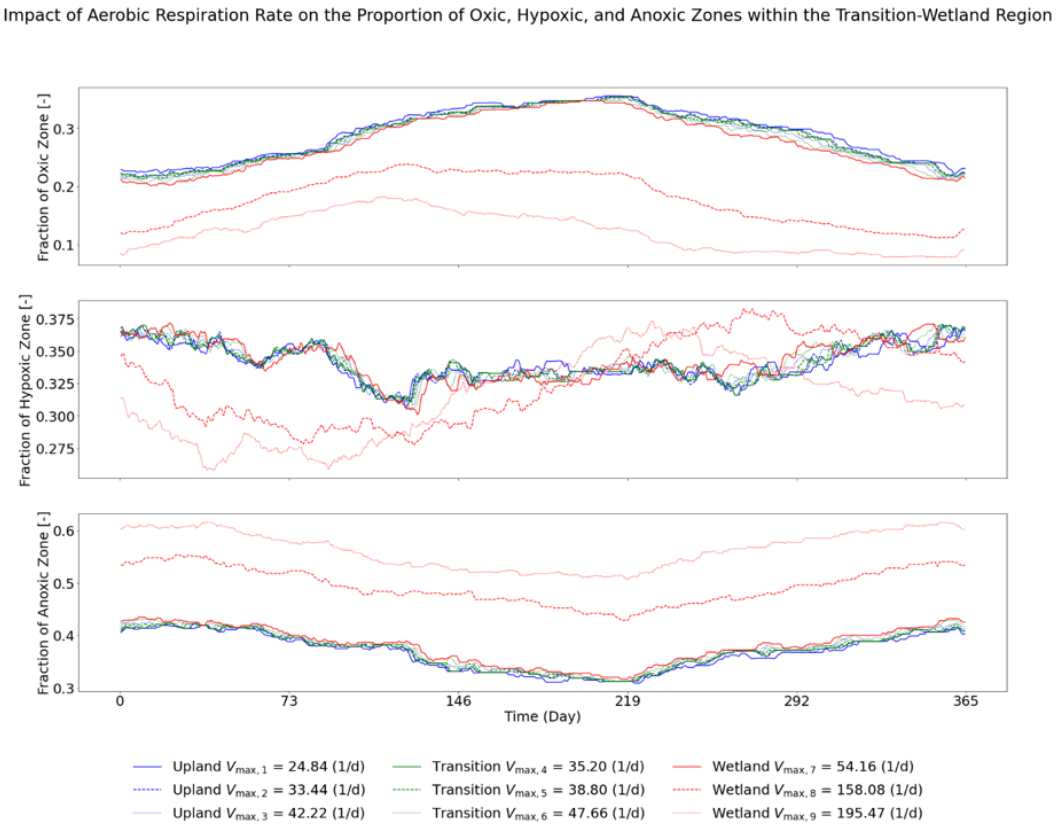

Figure 13: Three subfigures showcasing the distribution of oxic, hypoxic, and anoxic zones in the Transition-Wetland region. Each subfigure has nine lines representing different rate cases, demonstrating the changes in these fractions over time. The trend of the oxic, hypoxic, and anoxic zone ratios varies over time, reflecting the dynamic nature of oxygen availability within the wetland-transition region.

4 Limitations of Current Work and Future Work

In our current model, we constrained the maximum reaction rate constant of denitrification for all scenarios due to limited data availability. This approach was suitable for this study since aerobic respiration processes played a predominant role in our study as the cybernetic reaction approach allowed us to vary denitrification rates through the regulation component. However, similar to the variation observed in the maximum reaction rate of aerobic respiration across coastal TAIs, the relative parameters for denitrification should also exhibit variability. We have a sampling plan in place and will gather the necessary data to incorporate these variations in the coming year. This will enable us to conduct more accurate analyses in the future.

The estimation of the external DOC inputs was based on empirical equations that rely on rainfall intensity. A study conducted by [*O'Meara et al.*, 2019] employed the ELM and PFLOTRAN to simulate vegetation dynamics and update biogeochemical representations. In order to more precisely quantify the decomposition effects of plants on the entire ecosystem, we plan to integrate ELM into ATS-PFLOTRAN. This integration will enable the calculation of decomposition processes, such as litterfall, particulate organic carbon, and dissolved organic carbon, which are influenced by different plant types. These calculations will be performed locally and assigned to the corresponding domains, leading to more accurate estimations of decomposition processes within the model.

Using a selected 2-D transect in modeling flow and transport is inherently a limitation as it restricts the representation of 3-D solute movement in the field. This means that the model does not capture the lateral flow that occurs perpendicular to the transect. This limitation can affect the accuracy and completeness of the results. In particular, it has been found that the uphill water level does not have a significant impact on the downhill distribution and reaction of solutes. By examining the flow path shown in the supplementary information, it is apparent that the flow direction is from right to left in the left side of the domain, driven by the pressure gradient resulting from the topography difference. This flow direction can also influence the transport of solutes such as DOC and nitrate in groundwater. To better align with field measurement data and improve the accuracy of the model, we plan to incorporate a 3-D model in future simulations. This would allow for the inclusion of lateral flow and capture the full complexity of solute movement in three dimensions.

5 Summary and Conclusions

Complex interactions among hydro-biogeochemical processes in coastal TAIs are vital to regulating the coastal ecosystem. These interactions have a significant impact on carbon, nutrient, and redox processes. Therefore, understanding these intricate interactions is crucial for accurately predicting carbon cycling and effectively managing the water quality of these ecosystems. Our understanding of how hydraulic and ecological processes interact and influence biogeochemical processes in the coastal ecosystem remains incomplete, primarily due to limitations in modeling techniques. Here we analyzed the effects of four key factors on carbon cycling in the coastal TAIs: aerobic respiration rate, precipitation and flooding, ET, and external carbon sources using a newly integrated hydro-biogeochemical model with calibrated aerobic respiration rates supported by field-measured data.

Numerical simulations revealed the formation of active exchange flows and reaction hot spots at the TAIs as a result of the dynamic interaction between hydrological and biogeochemical processes. The coupled simulations of flow, reactive transport, and land surface processes have generated valuable insights on the consequences of extreme precipitation and sea level rise. We found that strong tidal flooding transports more oxygenated water to the transition zone of TAI, enhancing aerobic respiration, while heavy

precipitations transport more terrestrial-derived organic matter to the coastal TAI, depleting the oxygen in the system. Vegetation-induced ET also enhances the exchange fluxes across the TAI by altering the local hydraulic gradient.

While the formation of persistent active exchange zones is largely shaped by the site geomorphology and hydrology, the biogeochemical transformations in these zones is highly sensitive to reaction rate constants, which vary substantially across the TAI. The extent of the oxic, hypoxic, and anoxic zones differ significantly across the range of aerobic respiration rates. Understanding these relationships is crucial for the management and conservation of transitional areas and their associated ecosystem services.

Our results demonstrate the importance of considering multiple physical and biogeochemical processes in the study of coastal wetlands, as they indirectly and directly affect the carbon cycle and ecosystems in space and time. The results suggest that changes in the aerobic respiration rate, precipitation and flooding, ET, and external carbon sources can all have significant impacts on carbon cycling rates and the overall carbon balance of an ecosystem. These findings are important for understanding and managing the carbon cycle and its impact on climate change. The carbon cycle is a crucial process in the Earth's ecosystem, where carbon is continuously exchanged between the atmosphere, oceans, land, and living organisms. The balance of carbon in the atmosphere directly affects the Earth's climate, making it important to understand the factors that influence carbon cycling rates in ecosystems. While the results provide valuable insights into the system behavior, the findings of this study should be interpreted in the context of its exploratory nature., It is important to recognize that further research and field measurements are necessary to fully understand and validate these findings.

6 Open Research

In accordance with FAIR Data guidelines, we provide the following information regarding the availability of data and software used in this study. The data supporting this research can be found in the following repositories: Data and codes used in this paper are achieved in the ESS-DIVE (`https://data.ess-dive.lbl.gov/view/doi:10.15485/1986338` [*Li et al.*, 2023]) and figshare (`https://doi.org/10.6084/m9.figshare.c.6759357.v1` [*Ward and Moore*, 2023].

Acknowledgments

This research is supported by the U.S. Department of Energy (DOE), Office of Biological and Environmental Research (BER), as part of BER's Environmental System Science. This contribution originates from the Coastal Observations, Mechanisms, and Predictions Across Systems and Scales - Field, Measurements and Experiments (COMPASS-FME) project, a multi-institutional program led by Pacific Northwest National Laboratory (PNNL). PNNL is operated for DOE by Battelle Memorial Institute under contract DE-AC05-76RL01830. This research used the COMPASS Supercomputer for model simulations. This paper describes objective technical results and analysis. Any subjective views or opinions that might be expressed in the paper do not necessarily represent the views of the U.S. Department of Energy or the United States Government.

References

Andre, B., S. Molins, J. Johnson, and C. Steefel (2013), Alquimia, *Tech. rep.*, Lawrence Berkeley National Lab.(LBNL), Berkeley, CA (United States).

Assessment, M. E. (2005), *Ecosystems and human well-being: wetlands and water synthesis*, World Resources Institute, Washington, DC.

Bailey, V., J. Rowland, J. P. Megonigal, T. Troxler, J. DeForest, and D. Stover (2017a), Research priorities to incorporate terrestrial-aquatic interfaces in earth system models. workshop report, september 7-9, 2016, *Tech. rep.*, USDOE Office of Science (SC), Washington, DC (United States). Biological and ....

Bailey, V., A. Smith, M. Tfaily, S. Fansler, and B. Bond-Lamberty (2017b), Differences in soluble organic carbon chemistry in pore waters sampled from different pore size domains, *Soil Biology and Biochemistry*, *107*, 133–143.

Bauer, J. E., W.-J. Cai, P. A. Raymond, T. S. Bianchi, C. S. Hopkinson, and P. A. Regnier (2013), The changing carbon cycle of the coastal ocean, *Nature*, *504*(7478), 61–70.

Bhatla, R., S. Verma, R. Pandey, and A. Tripathi (2019), Evolution of extreme rainfall events over indo-gangetic plain in changing climate during 1901–2010, *Journal of Earth System Science*, *128*, 1–14.

Bianchi, T. S., X. Cui, N. E. Blair, D. J. Burdige, T. I. Eglinton, and V. Galy (2018), Centers of organic carbon burial and oxidation at the land-ocean interface, *Organic Geochemistry*, *115*, 138–155.

Boano, F., J. W. Harvey, A. Marion, A. I. Packman, R. Revelli, L. Ridolfi, and A. Wörman (2014), Hyporheic flow and transport processes: Mechanisms, models, and biogeochemical implications, *Reviews of Geophysics*, *52*(4), 603–679.

Casas-Ruiz, J. P., P. Bodmer, K. A. Bona, D. Butman, M. Couturier, E. J. Emilson, K. Finlay, H. Genet, D. Hayes, J. Karlsson, et al. (2023), Integrating terrestrial and aquatic ecosystems to constrain estimates of land-atmosphere carbon exchange, *Nature Communications*, *14*(1), 1571.

Chmura, G. L., S. C. Anisfeld, D. R. Cahoon, and J. C. Lynch (2003), Global carbon sequestration in tidal, saline wetland soils, *Global biogeochemical cycles*, *17*(4).

Cleveland, C. C., J. C. Neff, A. R. Townsend, and E. Hood (2004), Composition, dynamics, and fate of leached dissolved organic matter in terrestrial ecosystems: results from a decomposition experiment, *Ecosystems*, *7*, 175–285.

Coon, E. T., and P. Shuai (2022), Watershed workflow: A toolset for parameterizing data-intensive, integrated hydrologic models, *Environmental Modelling & Software*, *157*, 105,502.

Coon, E. T., J. D. Moulton, and S. L. Painter (2016), Managing complexity in simulations of land surface and near-surface processes, *Environmental modelling & software*, *78*, 134–149.

Coon, E. T., J. D. Moulton, E. Kikinzon, M. Berndt, G. Manzini, R. Garimella, K. Lipnikov, and S. L. Painter (2020), Coupling surface flow and subsurface flow in complex soil structures using mimetic finite differences, *Advances in Water Resources*, *144*, 103,701.

Costanza, R., R. d'Arge, R. de Groot, S. Farber, M. Grasso, B. Hannon, ..., and M. van den Belt (1997), The value of the world's ecosystem services and natural capital, *Nature*, *387*(6630), 253–260.

Cowardin, L. M., V. Carter, F. C. Golet, and E. T. LaRoe (1979), Classification of wetlands and deepwater habitats of the united states, *Tech. rep.*, U.S. Fish and Wildlife Service, Washington, DC.

Craft, C. (2007), Freshwater input structures soil properties, vertical accretion, and nutrient accumulation of georgia and us tidal marshes, *Limnology and oceanography*, *52*(3), 1220–1230.

Enguehard, L., N. Falco, M. Schmutz, M. E. Newcomer, J. Ladau, J. B. Brown, L. Bourgeau-Chavez, and H. M. Wainwright (2022), Machine-learning functional zonation approach for characterizing terrestrial–aquatic interfaces: Application to lake erie, *Remote Sensing*, *14*(14), 3285.

Erickson III, D. J., B. Sulzberger, R. G. Zepp, and A. T. Austin (2015), Effects of stratospheric ozone depletion, solar uv radiation, and climate change on biogeochemical cycling: interactions and feedbacks, *Photochemical & Photobiological Sciences*, *14*(1), 127–148.

Erwin, K. L. (2009), Wetlands and global climate change: the role of wetland restoration in a changing world, *Wetlands Ecology and management*, *17*(1), 71–84.

Fang, Y., T. Zheng, B. Guo, H. Zhan, H. Wang, X. Zheng, and M. Walther (2022), Transformation in the stability of tide-induced upper saline plume driven by transient external forcing, *Water Resources Research*, *58*(6), e2021WR031,331.

Flato, G. M. (2011), Earth system models: an overview, *Wiley Interdisciplinary Reviews: Climate Change*, *2*(6), 783–800.

Franklin, R. B., E. M. Morrissey, and J. C. Morina (2017), Changes in abundance and community structure of nitrate-reducing bacteria along a salinity gradient in tidal wetlands, *Pedobiologia*, *60*, 21–26.

Ganju, N. K., Z. Defne, T. Elsey-Quirk, and J. M. Moriarty (2019), Role of tidal wetland stability in lateral fluxes of particulate organic matter and carbon, *Journal of Geophysical Research: Biogeosciences*, *124*(5), 1265–1277.

Goll, D. S., V. Brovkin, B. Parida, C. H. Reick, J. Kattge, P. B. Reich, P. Van Bodegom, and Ü. Niinemets (2012), Nutrient limitation reduces land carbon uptake in simulations with a model of combined carbon, nitrogen and phosphorus cycling, *Biogeosciences*, *9*(9), 3547–3569.

Grande, E., B. Arora, A. Visser, M. Montalvo, A. Braswell, E. Seybold, C. Tatariw, K. Beheshti, and M. Zimmer (2022), Tidal frequencies and quasiperiodic subsurface water level variations dominate redox dynamics in a salt marsh system, *Hydrological Processes*, *36*(5), e14,587.

Hammond, G. E. (2022), The pflotran reaction sandbox, *Geoscientific Model Development*, *15*(4), 1659–1676.

Hammond, G. E., P. C. Lichtner, and R. Mills (2014), Evaluating the performance of parallel subsurface simulators: An illustrative example with pflotran, *Water resources research*, *50*(1), 208–228.

Hengl, T., J. Mendes de Jesus, G. B. Heuvelink, M. Ruiperez Gonzalez, M. Kilibarda, A. Blagotić, W. Shangguan, M. N. Wright, X. Geng, B. Bauer-Marschallinger, et al. (2017), Soilgrids250m: Global gridded soil information based on machine learning, *PLoS one*, *12*(2), e0169,748.

Hitchcock, J. N. (2020), Storm events as key moments of microplastic contamination in aquatic ecosystems, *Science of The Total Environment*, *734*, 139,436.

Kalev, S., and G. S. Toor (2020), Concentrations and loads of dissolved and particulate organic carbon in urban stormwater runoff, *Water*, *12*(4), 1031.

Kolka, R., C. Trettin, and L. Windham-Myers (2021), The importance of wetland carbon dynamics to society: insight from the second state of the carbon cycle science report, *Wetland Carbon and Environmental Management*, pp. 421–436.

Koshila Ravi, R., S. Anusuya, M. Balachandar, and T. Muthukumar (2019), Microbial interactions in soil formation and nutrient cycling, *Mycorrhizosphere and pedogenesis*, pp. 363–382.

Krauss, K. W., G. B. Noe, J. A. Duberstein, W. H. Conner, C. L. Stagg, N. Cormier, M. C. Jones, C. E. Bernhardt, B. Graeme Lockaby, A. S. From, et al. (2018), The role of the upper tidal estuary in wetland blue carbon storage and flux, *Global Biogeochemical Cycles*, *32*(5), 817–839.

Kuzyakov, Y., and E. Blagodatskaya (2015), Microbial hotspots and hot moments in soil: concept & review, *Soil Biology and Biochemistry*, *83*, 184–199.

LaFond-Hudson, S., and B. Sulman (2023), Modeling strategies and data needs for representing coastal wetland vegetation in land surface models, *New Phytologist*, *238*(3), 938–951.

Lal, A. W. (1998), Weighted implicit finite-volume model for overland flow, *Journal of Hydraulic Engineering*, *124*(9), 941–950.

Lawrence, D. M., R. A. Fisher, C. D. Koven, K. W. Oleson, S. C. Swenson, G. Bonan, N. Collier, B. Ghimire, L. van Kampenhout, D. Kennedy, et al. (2019), The community land model version 5: Description of new features, benchmarking, and impact of forcing uncertainty, *Journal of Advances in Modeling Earth Systems*, *11*(12), 4245–4287.

Lee, S., R. Dunn, R. Young, R. Connolly, P. Dale, R. Dehayr, C. Lemckert, S. McKinnon, B. Powell, P. Teasdale, et al. (2006), Impact of urbanization on coastal wetland structure and function, *Austral Ecology*, *31*(2), 149–163.

Li, B., X. Liu, M. H. Kaufman, A. Turetcaia, X. Chen, and M. B. Cardenas (2020), Flexible and modular simultaneous modeling of flow and reactive transport in rivers and hyporheic zones, *Water Resources Research*, *56*(2), e2019WR026,528.

Li, B., S. Pennington, J. H. Z. J. W. N. M.-P. A. Regier, P., and R. R (2023), Data, figures, animations, and scripts associated with the manuscript "integrated effects of site hydrology and vegetation on exchange fluxes and carbon cycling at the coastal terrestrial aquatic interface", doi:10.15485/1986338.

Linker, L. C., R. Dennis, G. W. Shenk, R. A. Batiuk, J. Grimm, and P. Wang (2013), Computing atmospheric nutrient loads to the chesapeake bay watershed and tidal waters, *JAWRA Journal of the American Water Resources Association*, *49*(5), 1025–1041.

Lu, M., E. R. Herbert, J. A. Langley, M. L. Kirwan, and J. P. Megonigal (2019), Nitrogen status regulates morphological adaptation of marsh plants to elevated co2, *Nature Climate Change*, *9*(10), 764–768.

Mattone, C., and M. Sheaves (2017), Patterns, drivers and implications of dissolved oxygen dynamics in tropical mangrove forests, *Estuarine, Coastal and Shelf Science*, *197*, 205–213.

McClain, M. E., E. W. Boyer, C. L. Dent, S. E. Gergel, N. B. Grimm, P. M. Groffman, S. C. Hart, J. W. Harvey, C. A. Johnston, E. Mayorga, et al. (2003), Biogeochemical hot spots and hot moments at the interface of terrestrial and aquatic ecosystems, *Ecosystems*, pp. 301–312.

McDowell, N. G., M. Ball, B. Bond-Lamberty, M. L. Kirwan, K. W. Krauss, J. P. Megonigal, M. Mencuccini, N. D. Ward, M. N. Weintraub, and V. Bailey (2022), Processes and mechanisms of coastal woody-plant mortality, *Global Change Biology*, *28*(20), 5881–5900.

Megonigal, J. P., M. Hines, and P. Visscher (2004), Anaerobic metabolism: linkages to trace gases and aerobic processes, *Biogeochemistry*.

Menendez, A., M. Tzortziou, P. Neale, P. Megonigal, L. Powers, P. Schmitt-Kopplin, and M. Gonsior (2022), Strong dynamics in tidal marsh doc export in response to natural cycles and episodic events from continuous monitoring, *Journal of Geophysical Research: Biogeosciences*, *127*(7), e2022JG006,863.

Michael, H. A., A. E. Mulligan, and C. F. Harvey (2005), Seasonal oscillations in water exchange between aquifers and the coastal ocean, *Nature*, *436*(7054), 1145–1148.

Mitsch, W. J., and J. G. Gosselink (2007), *Wetlands*, 4th ed., John Wiley & Sons.

Moore, W. S. (2010), The effect of submarine groundwater discharge on the ocean, *Annual review of marine science*, *2*, 59–88.

Mopper, K., D. J. Kieber, and A. Stubbins (2015), Marine photochemistry of organic matter: processes and impacts, *Biogeochemistry of marine dissolved organic matter*, pp. 389–450.

Nelson, N. G., R. Muñoz-Carpena, P. J. Neale, M. Tzortziou, and J. P. Megonigal (2017), Temporal variability in the importance of hydrologic, biotic, and climatic descriptors of dissolved oxygen dynamics in a shallow tidal-marsh creek, *Water Resources Research*, *53*(8), 7103–7120.

Oh, H., and J.-H. Choi (2022), Changes in the dissolved organic matter characteristics released from sediment according to precipitation in the namhan river with weirs: A laboratory experiment, *International Journal of Environmental Research and Public Health*, *19*(9), 4958.

Oleson, K., D. Lawrence, G. Bonan, M. Flanner, E. Kluzek, P. Lawrence, S. Levis, S. Swenson, P. Thornton, A. Dai, et al. (2010), Technical description of version 4.0 of the community land model (clm), ncar technical note, *National Center for Atmospheric Research, Boulder, CO, USA*.

Oleson, K., D. Lawrence, G. Bonan, B. Drewniak, M. Huang, C. Koven, S. Levis, F. Li, W. Riley, Z. Subin, et al. (2013), Technical description of version 4.5 of the community land model (clm)(ncar technical note no. ncar/tn-503+ str). citeseer, *National Center for Atmospheric Research, PO Box*, *3000*, 555.

O'Meara, T., B. Sulman, F. Yuan, P. E. Thornton, and P. Megonigal (2019), Integrating saltmarsh vegetation dynamics, hydrology, and biogeochemistry with the elm-pflotran interface, in *AGU Fall Meeting Abstracts*, vol. 2019, pp. B43H–2540.

Paerl, H. W., N. S. Hall, A. G. Hounshell, R. A. Luettich Jr, K. L. Rossignol, C. L. Osburn, and J. Bales (2019), Recent increase in catastrophic tropical cyclone flooding in coastal north carolina, usa: Long-term observations suggest a regime shift, *Scientific reports*, *9*(1), 10,620.

Patel, K. F., K. A. Rod, C. Norris, M. Kaufman, P. Megonigal, M. N. Weintraub, and V. L. Bailey (2022), Time to anoxia: Oxygen consumption in soils varies across a coastal gradient, in *AGU Fall Meeting Abstracts*, vol. 2022, pp. GC46D–08.

Radojević, M. (1986), Nitrite in rainwater, *Atmospheric Environment (1967)*, *20*(6), 1309–1310.

Regier, P., N. D. Ward, J. Indivero, C. Wiese Moore, M. Norwood, and A. Myers-Pigg (2021), Biogeochemical control points of connectivity between a tidal creek and its floodplain, *Limnology and Oceanography Letters*, *6*(3), 134–142.

Rich, J. J., O. R. Dale, B. Song, and B. B. Ward (2008), Anaerobic ammonium oxidation (anammox) in chesapeake bay sediments, *Microbial Ecology*, *55*(2), 311–320.

Richards, L. A. (1931), Capillary conduction of liquids through porous mediums, *Physics*, *1*(5), 318–333.

Rivett, M. O., S. R. Buss, P. Morgan, J. W. Smith, and C. D. Bemment (2008), Nitrate attenuation in groundwater: a review of biogeochemical controlling processes, *Water research*, *42*(16), 4215–4232.

Robinson, C. E., P. Xin, I. R. Santos, M. A. Charette, L. Li, and D. A. Barry (2018), Groundwater dynamics in subterranean estuaries of coastal unconfined aquifers: Controls on submarine groundwater discharge and chemical inputs to the ocean, *Advances in Water Resources*, *115*, 315–331.

Scott, R. L., T. E. Huxman, W. L. Cable, and W. E. Emmerich (2006), Partitioning of evapotranspiration and its relation to carbon dioxide exchange in a chihuahuan desert shrubland, *Hydrological Processes: An International Journal*, *20*(15), 3227–3243.

Seitzinger, S. P. (1994), Linkages between organic matter mineralization and denitrification in eight riparian wetlands, *Biogeochemistry*, *25*, 19–39.

Smith, A. J., and M. L. Kirwan (2021), Sea level-driven marsh migration results in rapid net loss of carbon, *Geophysical Research Letters*, *48*(13), e2021GL092,420.

Song, H.-S., and D. Ramkrishna (2011), Cybernetic models based on lumped elementary modes accurately predict strain-specific metabolic function, *Biotechnology and Bioengineering*, *108*(1), 127–140.

Song, X., X. Chen, J. Stegen, G. Hammond, H.-S. Song, H. Dai, E. Graham, and J. M. Zachara (2018), Drought conditions maximize the impact of high-frequency flow variations on thermal regimes and biogeochemical function in the hyporheic zone, *Water Resources Research*, *54*(10), 7361–7382.

Spalding, R. F., and M. E. Exner (1993), Occurrence of nitrate in groundwater—a review, *Journal of environmental quality*, *22*(3), 392–402.

Tank, S. E., J. B. Fellman, E. Hood, and E. S. Kritzberg (2018), Beyond respiration: Controls on lateral carbon fluxes across the terrestrial-aquatic interface, *Limnology and Oceanography Letters*, *3*(3), 76–88.

Thorne, C. R., and J. E. Williams (1997), The terrestrial-aquatic interface: a model for planning and managing the multiple uses of wetlands, *Wetlands Ecology and Management*, *4*(1), 47–60.

Trefry, M. G., and C. Muffels (2007), Feflow: A finite-element ground water flow and transport modeling tool, *Groundwater*, *45*(5), 525–528.

Triska, F. J., J. H. Duff, and R. J. Avanzino (1993), The role of water exchange between a stream channel and its hyporheic zone in nitrogen cycling at the terrestrial-aquatic interface, *Hydrobiologia*, *251*, 167–184.

Vymazal, J., and L. Kröpfelová (2008), *Wastewater treatment in constructed wetlands with horizontal sub-surface flow*, vol. 14, Springer science & business media.

Wang, H., B. Sun, X. Yu, Z. Xin, and G. Jia (2020), The driver-pattern-effect connection of vegetation dynamics in the transition area between semi-arid and semi-humid northern china, *Catena*, *194*, 104,713.

Ward, A. R. P. I. J. N. M. J., Nicholas. Myers-Pigg, and C. W. Moore (2023), Data for hou et al. quantifying drivers of methane hydrobiogeochemistry in a tidal river floodplain system., doi:https://doi.org/10.6084/m9.figshare.c.6759357.v1.

Ward, N. D., J. P. Megonigal, B. Bond-Lamberty, V. L. Bailey, D. Butman, E. A. Canuel, H. Diefenderfer, N. K. Ganju, M. A. Goñi, E. B. Graham, et al. (2020), Representing the function and sensitivity of coastal interfaces in earth system models, *Nature communications*, *11*(1), 2458.

Waska, H., J. Greskowiak, J. Ahrens, M. Beck, S. Ahmerkamp, P. Böning, H.-J. Brumsack, J. Degenhardt, C. Ehlert, B. Engelen, et al. (2019), Spatial and temporal patterns of pore water chemistry in the inter-tidal zone of a high energy beach, *Frontiers in Marine Science*, *6*, 154.

Wohl, E., S. N. Lane, and A. C. Wilcox (2015), The science and practice of river restoration, *Water Resources Research*, *51*(8), 5974–5997.

Xin, P., A. Wilson, C. Shen, Z. Ge, K. B. Moffett, I. R. Santos, X. Chen, X. Xu, Y. Y. Yau, W. Moore, et al. (2022), Surface water and groundwater interactions in salt marshes and their impact on plant ecology and coastal biogeochemistry, *Reviews of Geophysics*, *60*(1), e2021RG000,740.

Xu, Z., S. Molins, D. Svyatskiy, I. Özgen-Xian, D. Dwivedi, E. R. Siirila-Woodburn, J. D. Moulton, and C. I. Steefel (2019), Understanding integrated hydrology and geochemistry processes in a mountainous watershed using the advanced terrestrial simulator (ats), in *AGU Fall Meeting Abstracts*, vol. 2019, pp. H21J–1882.

Yabusaki, S. B., A. N. Myers-Pigg, N. D. Ward, S. R. Waichler, A. Sengupta, Z. Hou, X. Chen, Y. Fang, Z. Duan, J. A. Serkowski, et al. (2020), Floodplain inundation and salinization from a recently restored first-order tidal stream, *Water Resources Research*, *56*(7), e2019WR026,850.

Zhang, Y., D. Svyatsky, J. C. Rowland, J. D. Moulton, Z. Cao, P. J. Wolfram, C. Xu, and D. Pasqualini (2022), Impact of coastal marsh eco-geomorphologic change on saltwater intrusion under future sea level rise, *Water Resources Research*, *58*(5), e2021WR030,333.

Zheng, J., and P. V. Doskey (2015), Modeling nitrous oxide production and reduction in soil through explicit representation of denitrification enzyme kinetics, *Environmental science & technology*, *49*(4), 2132–2139.